Hindawi
Adsorption Science & Technology
Volume 2021, Article ID 5201497, 19 pages
https://doi.org/10.1155/2021/5201497

Research Article

Preparation of Hierarchical Structure Au/ZnO Composite for Enhanced Photocatalytic Performance: Characterization, Effects of Reaction Parameters, and Oxidizing Agent Investigations

Anh-Tuan Vu,[1] **Thi Anh Tuyet Pham**,[1] **Xuan Truong Do**,[1] **Van Anh Tran**,[1] **Van Duong Le**,[1] **Duc Duc Truong**,[1] **The Huu Nguyen**,[2] **and Minh Viet Nguyen**[2]

[1]*School of Chemical Engineering, Hanoi University of Science and Technology, Vietnam*
[2]*Faculty of Chemical Technology, Hanoi University of Industry, Vietnam*

Correspondence should be addressed to Anh-Tuan Vu; tuan.vuanh@hust.edu.vn and Minh Viet Nguyen; minhviet@haui.edu.vn

Received 6 August 2021; Revised 21 October 2021; Accepted 23 October 2021; Published 18 November 2021

Academic Editor: Amit Kumar

Zinc oxide (ZnO) has been shown as a potential photocatalyst under ultraviolet (UV) light but its catalytic activity has a limitation under visible (Vis) light due to the wide bandgap energy and the rapid recombination of electrons and holes. Thus, hierarchical structure Au/ZnO composites were fabricated by the hydrothermal method and chemical reduction method for enhanced photocatalytic performance under visible light. As-prepared composites were characterized by UV-vis diffuse reflectance spectra (DR/UV-Vis), field emission scanning electron microscope (FESEM), energy-dispersive X-ray spectroscopy (EDS), transmission electron microscopy (TEM), X-ray diffraction (XRD), Fourier transform infrared spectroscopy (FT-IR), and electron paramagnetic resonance (EPR). The Au/ZnO-5 composite showed the highest adsorption among as-prepared samples in the range of 250-550 nm, having bandgap energy of 0.13 eV. Au nanoparticles of about 3-5 nm were well dispersed on hierarchical flower ZnO with approximately 10-15 μm. The EPR signal at $g = 1.965$ on both ZnO and Au/ZnO samples was attributed to oxygen vacancy Vo•, but the presence of Au led to a decrease in signal strength of Au/ZnO composite, showing the degradation efficiency (DE) and reaction rate of 99.2% and 0.109 min^{-1}, respectively; these were larger than those of other samples. The effects of reaction parameters and oxidizing agents on photocatalytic performance were investigated and showed that the presence of H_2O_2 and O_2 could improve the reaction of composite. In addition, the kinetic and photocatalytic mechanism of tartrazine (TA) on catalysts were studied by the first-order kinetic model and characterized analyses.

1. Introduction

With the development of science and technology techniques, nanomaterials are being widely studied for many potential applications in medicine, environment, and industrialization. Nanoparticles are the simplest form of structures with size in the range of $(1 \div 100)$ nanometer that allows getting more multipurpose properties than block structures, especially for metal nanoparticles [1]. Recently, gold nanoparticles have attracted the attention of researchers for the reasons of nontoxic, high chemical and physical stability, easily perform surface functions with organic molecules, and countless optical properties associated with surface plasmon resonance [2]. The condition for resonance phenomenon is the frequency of the exciting light up to the oscillation frequency of the free electronic system on the metal surface. Au nanoparticles have resonance frequencies within the visible radiation area. Thus, they will strongly absorb visible light including solar light and causing the color effect [3]. Moreover, since the high interaction ability on the surface of other materials, the Au nanoparticles are commonly used as an agent to get the mutagenic properties within the catalysis, polymer, semiconductor, and medicine fields [4–7].

Environmental pollution is becoming a hot issue for over the world. The growing pollution in developing countries along with the development of industry and economy has caused serious pollution of water sources. It leads to significant impacts on human health and creates favorable conditions for the development of disease. The organic compounds in wastewater from industries like mining, oil refining, paper, paint, and textile plants are persistent and toxic. This is a challenging issue for the development of industry and economy. The conventional methods such as flocculation, adsorption, membrane process, and biological and chemical techniques [8–10] have been extensively used for the wastewater treatment, but their efficiencies have been not satisfactory to the practical technology for the treatment of wastewater containing multifarious contaminants, which are difficult to biodegrade [11, 12]. Meanwhile, semiconductor metal oxides emerge as a good candidate for the removal of persistent organic compounds in wastewater because of their efficiency in photocatalytic process. Under the irradiation of light, electrons from the valence band (VB) can jump into the conduction band (CB), leading to hole (h^+) generation in the VB. The electrons and holes play an important role in the redox process of organic pollutants [13]. They interact with O_2 and H_2O adsorbed on the surface of nanoparticles to create $\bullet O_2^-$ and •OH free radicals, which have strong oxidizing properties and are capable of decomposing organic substances into intermediate and final products of CO_2 and H_2O [14, 15]. Besides, metal oxide photocatalysts have been widely used on an industrial scale due to their environmental friendliness and high durability.

ZnO, a semiconductor oxide of n-type, has been widely utilized in numerous catalytic processes due to its specific properties like low cost, stability, and nontoxicity to the environment [16–18]. Hence, it is believed that ZnO is one of the promising multifunctional semiconductors for photocatalysis application in waste water treatment [19]. Zinc oxide has various morphologies depending on the synthesis method such as nanorods [20], nanowires [21], nanospheres [22], nanosheets [23], flower-like [24], hexagonal pyramid-like [25], and nanoparticles [26] which strongly affected the performance of catalyst [27]. However, the limitation of choosing ZnO as a photocatalyst is that it is most active in (<385 nm), which accounts for about 5% of sunlight, because of its wide bandgap energy (3.37 eV) and exciton binding energy (60 meV) [18]. In addition, the recombination between electrons and holes in bare ZnO takes place rapidly. These are the huge restrictions in the practical applications of ZnO photocatalyst. Therefore, improving the photocatalytic efficiency in the visible light region is a goal of scientists.

To overcome these disadvantages of ZnO, many methods have been proposed such as doping/codoing by metal oxides (Fe_2O_3, SnO_2, MnO_2, or CuO) [28, 29], precious metals (Au, Ag, Pt, or Pd) [30–32], metals (Fe, Mn, Ni, or Co) [33, 34], nonmetals (N, P, C, or S) [35, 36], or forming heterostructures with other semiconductors [37] to enhance the mobility of electrons and holes, prevent the recombination between them, and expand the light absorption region. Amongst them, doping ZnO nanomaterials by noble metals is the most suitable method because it could improve the photocatalytic activity of the semiconductor through these three pathways above at the same time. Several studies have demonstrated that the Schottky barrier will be formed when precious metal nanoparticles are directly anchored on the surface of ZnO [26, 38, 39]. Since the conduction band energy level of ZnO is larger than the Fermi energy of the precious metal, the separation of charge carriers is enhanced. Furthermore, due to the surface plasmon resonance (SPR) of the precious metal particles, ZnO can extend the absorption to the visible light region, leading to its enhanced catalytic activity under sunlight [14, 40, 41].

For enhancing photocatalysis and studying the effects of oxidizing agents on photocatalytic efficiency, the flower-like Au/ZnO structures were synthesized by the hydrothermal method and reduction method, which used the reducing agent of sodium citrate. The structure of the materials and the surface interactions that affect photocatalytic efficiency were investigated. The effects of reaction conditions like solution pH, catalyst dosage, concentration of TA, and light source and oxidizing agents (H_2O_2 and O_2) were evaluated by decomposition of dyes under visible light. Furthermore, the kinetics of the photocatalytic process was simulated according to the first-order kinetics equation.

2. Materials and Methods

2.1. Materials. Zinc nitrate hexahydrate ($Zn(NO_3)_2.6H_2O$, 99.5%), urea ($(NH_2)_2CO$, 99.5%), gold (III) chloride tetrahydrate ($HAuCl_4.4H_2O$, 99%), and sodium citrate ($Na_3C_6H_5O_7$, 99%) were purchased from China; tartrazine (99%), Janus Green B (99%), Congo red (99%), and methylene blue (99%) were obtained from Sigma-Aldrich.

2.2. Preparation of Hierarchical Flower-Like ZnO. The flower-like ZnO was prepared by the facile hydrothermal method [24]. Normally, 4.4623 g of $Zn(NO_3)_2.6H_2O$ and 1.8018 g of urea were poured into 100 mL of distilled water under stirring for 30 min to form a transparent mixed solution. Then, it was transferred into an autoclave at 90°C. After 24 h, the precipitate was filtered, washed with distilled water and ethanol several times, and dried at 90°C for 24 h. The ZnO powders were obtained after calcining the precipitate at 400°C for 2 h with a heating rate of 2°C/min. The formation of ZnO was described by the following equations.

$$
\begin{aligned}
(NH_2)_2CO + 3H_2O &\longrightarrow 2NH_3H_2O + CO_2 \\
NH_3.H_2O &\longrightarrow NH_4^+ + OH^- \\
CO_2 + OH^- &\longrightarrow CO_3^{2-} + H_2O \\
4Zn^{2+} + CO_3^{2-} + 6OH^- + H_2O &\longrightarrow Zn_4(CO_3)(OH)_6.H_2O \\
Zn_4(CO_3)(OH)_6.H_2O &\xrightarrow{t^o} 4ZnO + CO_2 + 4H_2O
\end{aligned}
\tag{1}
$$

2.3. Synthesis of Au/ZnO Composite. Au/ZnO composites were facially fabricated by the reduction of acid chloroauric by sodium citrate; the synthesis procedure is shown in

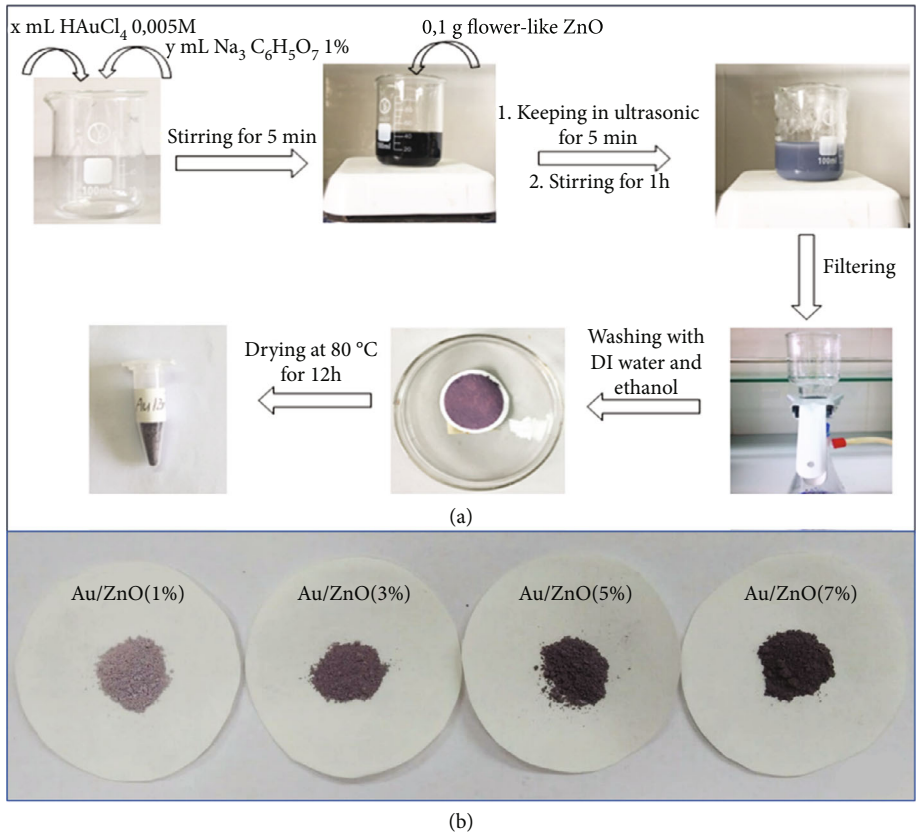

Figure 1: (a) The synthesis procedure of Au/ZnO composite and (b) the color change of Au/ZnO composites with the difference of Au contents.

Figure 1(a). First, the certain volumes of $HAuCl_4$ 0.005 M and $Na_3C_6H_5O_7$ 1% solutions were stirred together for 5 min. 0.1 g of ZnO sample was added to the solution and sonicated for 5 min and then stirred for 1 h to obtain a purple precipitate. It was filtered and washed with distilled water and ethanol to remove impurity ions and then dried at 80°C in the air for 12 h to obtain Au/ZnO-x composite where x was the Au content (1, 3, 5, and 7%) adjusted by varying the volumes of $HAuCl_4$ 0.005 M and $Na_3C_6H_5O_7$ 1%. The color of the Au/ZnO samples became darker when the Au content increased as seen in Figure 1(b).

2.4. Characterization. The XRD pattern was analyzed by a Bruker D8 Advance diffractometer (Germany) with Cu K_α irradiation (40 kV, 40 mA) to investigate the crystalline phase of samples. The morphology and size of the samples were observed by transmission electron microscopy (TEM, JEM-2010), emission scanning electron microscopy (FE-SEM, JEOL-7600F), and energy dispersive X-ray spectroscopy (EDS, JEOL-7600F). UV-vis diffuse reflectance spectra (DR/UV-vis) of the as-synthesized samples were measured on the UV-Vis spectrometer (Avantes). The FT-IR spectra were measured by Fourier transform infrared spectroscopy (FT-IR, Madison, WI, USA). The paramagnetic defect was analyzed by EPR spectroscopy (Bruker EMX Micro X).

2.5. Photocatalytic Test. The experiments were conducted by the batch reactor. A 250 mL glass beaker containing a specific concentration of dye was adjusted in pH by HCl and NaOH solutions; a specific amount of catalyst was added into the beaker and sonicated for 5 min. The mixture was left within the dark for 30 min to achieve the adsorption/desorption equilibrium and then placed under the Hg lamp 250 W with the light source intensity of 13450 Lux. At intervals, a little of the mixture from the beaker was filtered by a syringe filter (0.45 μm PTFE membrane) to extrude the catalyst. The concentration of dye was determined by UV-Vis method (Agilent 8453 instrument). The rate constant, degradation efficiency (DE), and degradation capacity (DC) of dyes were calculated by the subsequent equations:

$$\ln \frac{C_0}{C_t} = kt,$$
$$\mathrm{DE}\,(\%) = \frac{C_0 - C_t}{C_0} \times 100, \quad (2)$$
$$\mathrm{DC}\left(\frac{\mathrm{mg}}{\mathrm{g}}\right) = \frac{(C_0 - C_t) \times V}{m}.$$

where k is the pseudo-first-order rate constant; the k value was calculated from the slope of the $\ln(C_0/C_t) - t$ plots; C_0 and C_t are the concentrations of dye at initial ($t = 0$) and time t (min), respectively; V is the volume of dye solution (L); and m is the mass of the adsorbent (g).

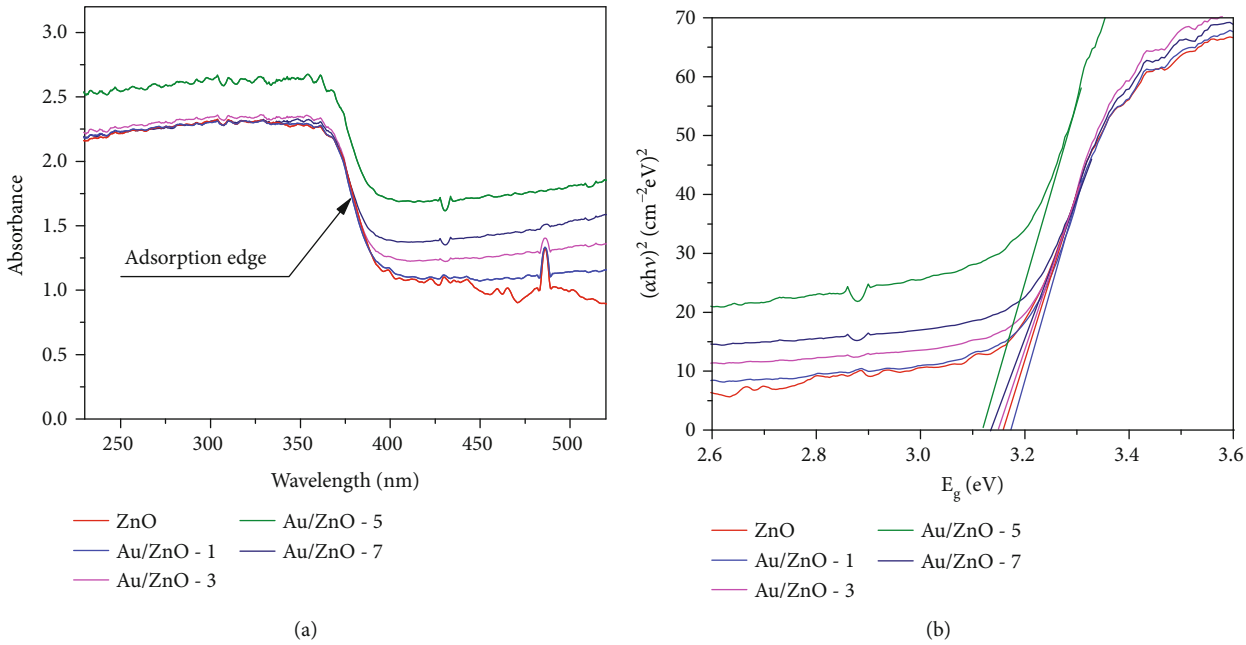

FIGURE 2: (a) DR/UV-vis and (b) Tauc's plots of the samples.

2.6. Determination of pH_{PZC}. The pH_{PZC} of the Au/ZnO sample was measured by the pH drift method. Initially, a 250 mL beaker containing 100 mL of 10 mg/L TA solution was adjusted to the pH solution values from 2 to 11 by HCl 0.1 M or NaOH 0.1 M solutions. Next, 0.05 g of Au/ZnO sample was poured into the beaker and stirred for 24 h at room temperature, then the final pH (pH_{final}) value was measured. The plot of pH_{final} versus $pH_{initial}$ will intersect the $pH_{initial}$ line at a point where it was defined as the pH_{PZC} of the catalyst.

3. Results and Discussion

3.1. Physicochemical Characterization. Figure 2 shows the DR/UV-vis and Tauc's plots of the ZnO and Au/ZnO samples. The presence of Au led to an increase in the absorption of Au/ZnO composites. The adsorptions of composites at Au content of 1, 3, and 7 wt.% were higher than that of the bare ZnO at the wavelength above 400 nm, although their adsorptions were like that of bare ZnO at lower than 380 nm, showing a similar adsorption edge, whereas the Au/ZnO-5 sample showed the highest adsorption among as-prepared composites at 250-500 nm in Figure 2(a). The bandgap energies (E_g) of the materials were determined by Tauc's method [17]:

$$(\alpha h\nu)^2 = A.(h\nu - E_g), \quad (3)$$

where α, h, ν, A, and E_g are absorption coefficient, Planck constant, light frequency, proportionality constant, and bandgap energy, respectively; the plots are showed in Figure 2(b). The E_g of bare ZnO (3.15 eV) was lower than that of Au/ZnO–1 (3.17 eV) but larger than those of other composites, which were 3.14, 3.12, and 3.13 eV for Au/ZnO–3, Au/ZnO–5, and Au/ZnO–7, respectively. It can be predicted that the uniform distribution and small content of Au in flower-like ZnO structure are the causes of the reduction in bandgap energy of the composite. As a result, the deposition of Au at a higher 3 wt.% in the composite led to reducing the bandgap energy and enhancing photocatalytic activity of composite under visible light irradiation. Also, it was expected that Au/ZnO-5 has the fastest decomposition rate for organic compounds.

Morphology and elemental map of samples are presented in Figure 3. The ZnO looked like a uniform flower with a hierarchical structure at size of approximately 10-15 μm (Figure 3(a)). The ZnO microstructure was composed of many thin petals made of oxide nanoparticles of about 30-40 nm, and there were many holes formed on the petals (Figures 3(b) and 3(c)). The size and shape of the Au/ZnO composite are similar to bare ZnO but the petals became denser due to the deposition of Au content in composite, in Figures 3(d)–3(f). Also, the good distribution of Zn, Au, and O elements was observed in Figures 3(g)–3(i), where there was no concentration of any elements. These were further evidenced by the color of the SEM/EDS image (Figure 3(j)) and the Zn, O, and Au contents of 51.3, 48.6, and 0.1%, respectively (Figure 3(k)).

The TEM results of samples are presented in Figure 4. The particle size of ZnO was about 20-50 nm (Figures 4(a) and 4(b)). Additionally, the Au nanoparticles of about 3-5 nm were well loaded and dispersed on microstructure ZnO as seen in (Figures 4(c) and 4(d)). This observation was in accordance with the SEM results above. It was expected to increase the catalytic performance of the composite.

The analytical results of the crystalline phase of as-prepared samples are shown in Figure 5. The intense peaks of bare ZnO at $2\theta = 31.7^\circ$, 34.4°, 36.2°, 47.5°, 56.6°, 62.8°, and 67.9° were associated with (100), (002), (101), (102), (110), (103), (112), and (201) plane, respectively, which

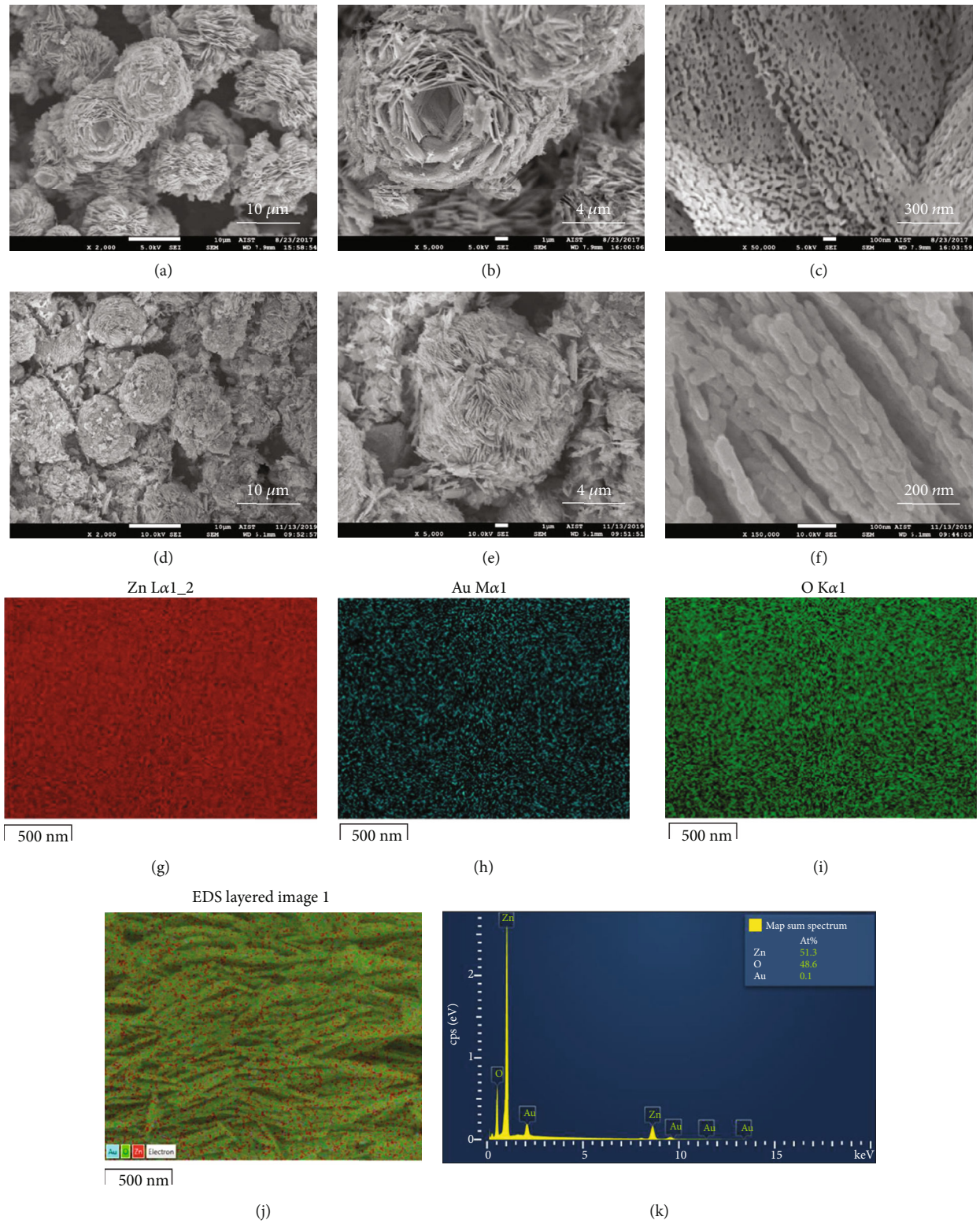

FIGURE 3: (a, b) SEM images of flower-like ZnO with the different scale bars, (d–f) SEM images of Au/ZnO-5 composite different scale bars, (g–i) Zn, Au, and O elemental map images, (j) SEM/EDS image, and (k) EDS spectrum Au/ZnO-5 composite.

proved the diffraction of hexagonal wurtzite structure of ZnO with lattice parameters in accordance with the reported data JCPDS file No. 36-1451 [42, 43]. The peaks of Au were not detected in Au/ZnO-5 composite although it was observed by SEM, EDS, and TEM images (Figures 3 and 4). This was possibly assigned to the low content and small particle size of Au [44]. However, the peak intensity of ZnO was decreased with adding Au into the composite.

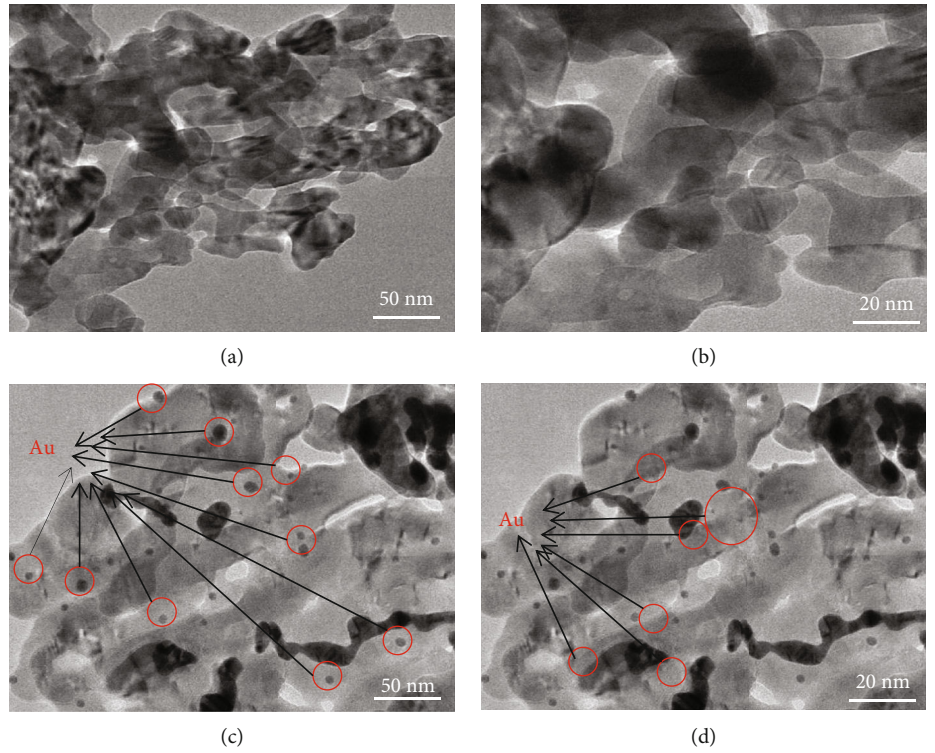

Figure 4: TEM images of (a, b) bare ZnO and (c, d) Au/ZnO-5 composite with the different scale bars.

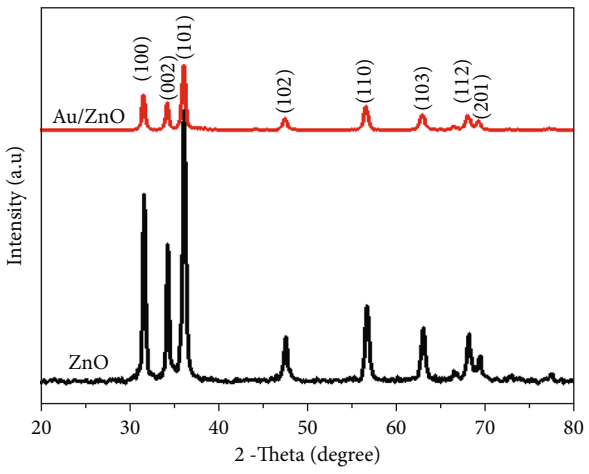

Figure 5: XRD patterns of bare ZnO and Au/ZnO-5 composite.

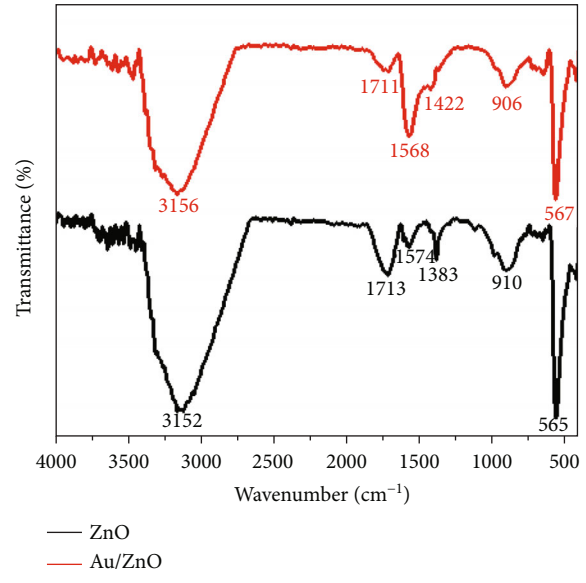

Figure 6: IR spectra of bare ZnO and Au/ZnO-5 composite.

The average crystallite size (D) of the nanoparticles was calculated from X-ray line broadening of the diffraction peaks by using Scherrer's equation:

$$D = \frac{K\lambda}{\beta \cos\theta}, \tag{4}$$

where K is a dimension shape factor, a typical value of about 0.9, λ is the wavelength of X-ray used (1.5405 Å), β is the angular peak width at half maximum in radians, and θ is Bragg's diffraction angle. As the result, the average crystal sizes of ZnO and Au/ZnO-5 were 8 and 15 nm, respectively. The slight reduction in the crystallinity and crystal size could be attributed to either breakdown from stirring during synthesis of Au/ZnO or the distortion by the foreign impurity of Au in the host lattice ZnO.

The FT-IR spectra of samples are shown in Figure 6. The strong bands at 3152 and 3156 cm^{-1} in both samples might be specified to O-H stretching vibration of absorbed water (H-O-H) [10]. The bands at 1574 of ZnO and 1568 cm^{-1} of Au/ZnO-5 might be attributed to the C=O bond [45]. The small band at 1713, 1383, and 910 cm^{-1} were associated with the vibration of O-H bond of Zn-O-H [24]. When Au was

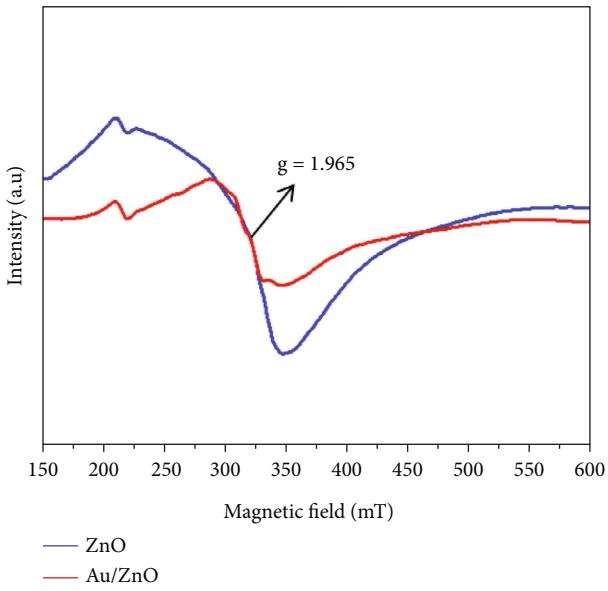

Figure 7: EPR spectra of bare ZnO and Au/ZnO-5 composite.

added into the composite, the intensity of bands was lowered whereas the band at 1574 cm^{-1} was more intense. In addition, the vibration bands in 1713 and 910 cm^{-1} were moved to a smaller wavenumber but the band at 1383 cm^{-1} was moved to a larger wavenumber. The strong bands at 567 and 565 cm^{-1} of ZnO and Au/ZnO-5 composite, respectively, were attributed to the Zn-O vibration in both samples [32].

Electron magnetic resonance (EPR) is a highly sensitive analytical technique for the detection of unpaired electrons and oxygen vacancies of Vo (+2 charge state), Vo• (+1 charge state), and Vo•• (0 charge state). Vo was rarely detected in ***n***-type ZnO, while Vo•• was easy to generate because of its low formation energy [39]. As shown in Figure 7, the signal at $g = 1.965$ on both ZnO and Au/ZnO-5 samples was attributed to oxygen vacancy Vo• [46], but the presence of Au led to a decrease in signal strength of Au/ZnO composite. This could be explained that the electrons of Au nanoparticles were transferred to ZnO and then paired with the lone electrons in Vo•, leading to the formation of paramagnetic Vo••. Which was the reason for the decrease in the recombination of electrons and holes. It was expected an increase in the photocatalytic ability of Au/ZnO composite.

3.2. Degradation of Dyes

3.2.1. Effect of Au Content on the Degradation of TA. Figure 8 shows the photocatalytic reaction of TA in Au/ZnO composites at the difference of Au contents. The reaction rate of TA in bare ZnO in the initial 10 min was faster but its DC in 30 min was lower than those of Au/ZnO-1, exhibiting the DEs of 59.3 and 79.1% for bare ZnO and Au/ZnO-1, respectively. Meanwhile, the DCs and reaction rates of TA in other composites were larger than those of bare ZnO. The DE and rate constant raised to 99.2% and 0.109 min^{-1}, respectively, when Au content increased to 5 wt.%. However, at Au content higher than 5 wt.%, the DE and reaction rate were lowered, showing 94.7% and 0.086 min^{-1}, respectively, for Ag/ZnO-7 composite. These results were in complete agreement with the results of the DR/UV-Vis spectrum, bandgap energy, and EPR analysis above, where the composite loaded Au at 5 wt.% was found to be the most efficient catalyst among as-prepared composites. As seen from previous research results [26], it can be realized that Au can enhance the catalytic ability of the composite at lower content than Ag.

3.2.2. Effect of pH Value of the Solution on the Degradation of TA. In each process of treating the organic matter in wastewater, the pH of the solution will play an important role because it affects not only the surface charge of the catalyst but also the ionization and structure of the pollutants. A wide pH range of 2.0–11.0 was selected for the study, while other conditions remained (catalyst dosage of 0.5 g/L, TA concentration of 10 mg/L, and light irradiation of Hg lamp 250 W). The results are shown in Figure 9.

The reaction of TA in Au/ZnO-5 composite at the pH value of 2.0 was relatively low; the DE in 30 min and the reaction rate were about 3% and 0.002 min^{-1}, respectively. The DE and reaction rate sharply increased to 99.2% and 0.109 min^{-1}, respectively, when solution pH increased to 6.0. These were lowered to 94.5% and 0.066 min^{-1} at the solution pH of 9.0. However, at solution pH of 11.0, the DE and reaction rate increase; these achieved 100% and 0.155 min^{-1}, respectively, as seen in Figures 9(a) and 9(b).

ZnO can be protonated in acidic media ($ZnO_{(s)} + 2H^{+}_{(aq)} \longrightarrow Zn^{2+}_{(aq)} + H_2O$). Therefore, the catalytic performance of ZnO could be neglected, at the pH of 2.0. However, in an alkaline medium, the catalytic performance was significantly enhanced because of the enhanced formation of •OH radicals from OH^- ions on the surface of the catalyst as well as in the reaction solution. As the result, at the pH of 11.0, the DC at 10 min and 30 min achieved 12.1 and 20.1 mg/g, respectively, showing greater magnitude than other pH values as seen in Figure 9(c). However, adjustment of an aqueous solution to a high pH value will have a limitation in treating the secondary wastewater because it must be neutralized before being discharged into the environment. Moreover, at high pH value, the ZnO can be dissolved ($ZnO(s) + 2OH^-_{(aq)} \longrightarrow ZnO_2^-{}_{(aq)} + H_2O$).

The pH of the solution influences the surface charge of the nanoparticles and changes the adsorption of organic substances on its surface. In the previous report, the pH point of the zero charges (pH_{PZC}) of ZnO was 9.0 [47]; the pH_{PZC} of the Au/ZnO-5 composite was reduced to 7.4 (Figure 9(d)) due to the deposition of Au. At pH 6.0, lower than the pH_{PZC} of the composite, the surface of the catalyst was positively charged due to the adsorption of H^+ ions; the TA dyes anions could be effectively adsorbed on the surface of the catalyst, increasing its catalytic efficiency. In addition, the pH_{final} at solution pH of 6.0 was higher than those of other solution pH values (Figure 9(d)). As the result, the anion TA dye could be efficiently adsorbed on the catalytic surface. Therefore, the dye degradation was significantly enhanced, showing the DCs of 10 and 30 min were 10.2 and 19.6 mg/g, respectively. When the pH of the solution

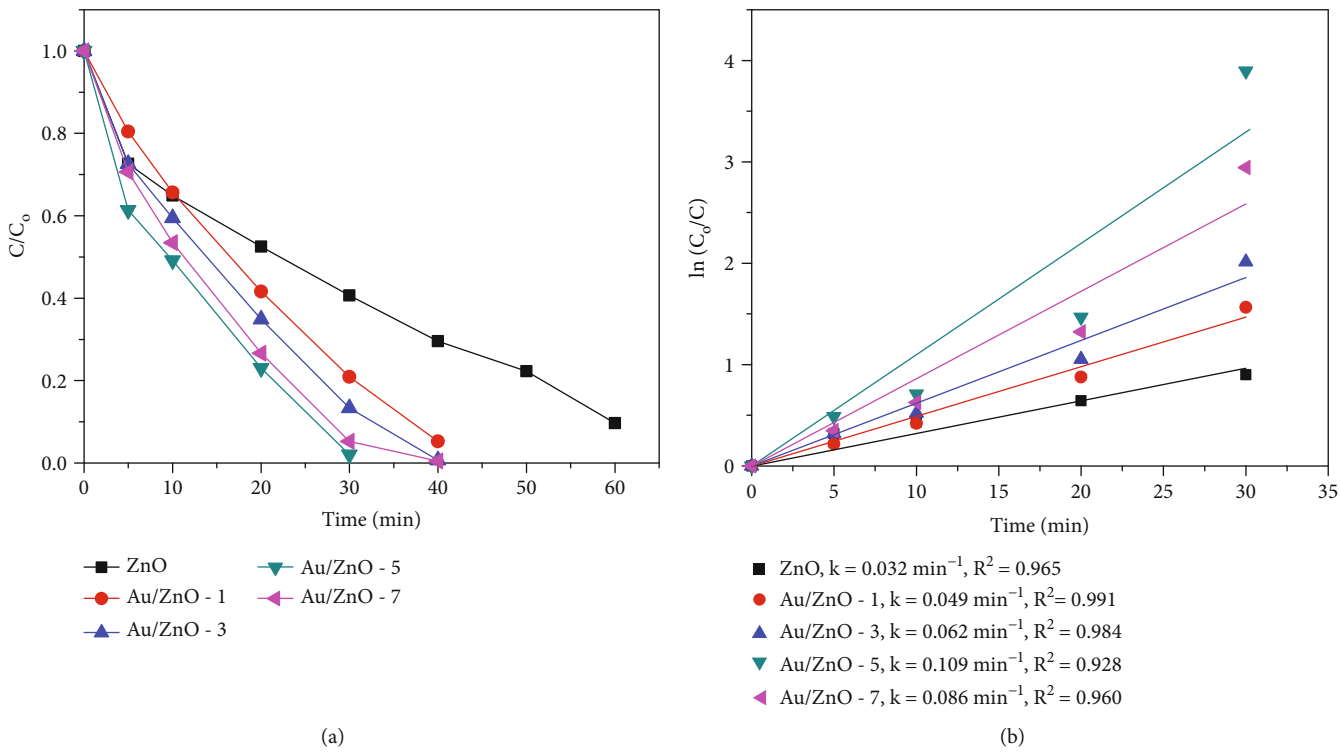

Figure 8: (a) Photocatalytic degradation of TA in ZnO and Au/ZnO composites at the different Au contents and (b) the kinetic curves. The reaction conditions: TA concentration of 10 mg/L, catalyst dosage of 0.5 g/L, pH solution of 6.0, and Hg lamp 250 W.

was higher than pHzpc, where the surface of the ZnO particles could be negatively charged by absorbing OH^- ions, it interfered with the adsorption of TA; however, the enhancement of the formation process of •OH radicals remained dominant, which resulted in increasing the catalytic efficiency at high pH values.

3.2.3. Effect of Initial TA Concentration. The concentration of TA from 5 to 20 mg/L was selected to demonstrate the effect of dye concentration on catalytic performance. The results were shown in Figure 10. The reaction rate at the initial TA concentration of 5 mg/L was faster than that of 10 mg/L, showing 0.159 and 0.109 min^{-1} for 5 and 10 mg/L, respectively. The DE in 30 min at both concentrations approached 100%, but the DC in 10 and 30 min at 10 mg/L was larger than those of 5 mg/L. When the initial TA concentration increased, the DE and reaction rate were relatively decreased. At the initial concentration of 20 mg/L, the degradation was completed in a remarkable time (80 min), and the reaction rate was 0.023 min^{-1}.

The decrease of DE and the reaction rate can be explained by the following reasons: (1) as the concentration of TA increased, the TA molecule shielded the photons before they reached the surface of the catalyst, and the generation of •OH and $•O_2^-$ radicals was reduced leading to reduced catalyst efficiency. (2) Alternatively, the number of TA molecules adsorbed on the catalyst surface increased with increasing dye concentration. The number of active sites of the catalyst surface was decreased, leading to a decrease in the reaction rate. (3) Otherwise, when the concentration of TA increased, the intermediate products would increase due to the catalytic degradation of the TA molecule creating competition between TA molecules and the intermediate products, while the total number of active sites remained constant for a fixed catalyst dosage. These results adversely affected the DE and reaction rate of TA on the catalyst. Although the high initial concentration of TA reduced the degradation yield and reaction rate, the DC values at 10 mg/L for 10 and 30 min were 10.1 mg/g and 19.6 mg/g, respectively. These exhibited a larger magnitude than the other concentrations (as shown in Figure 10(c)).

3.2.4. Effect of Catalyst Dosage. The experiments were carried out with selected catalyst dosages (0.25, 0.5, 0.75, and 1.0 g/L) to demonstrate their effect on catalyst performance; the results are presented in Figure 11. At the catalyst dosage of 0.25 g/L, the DE in 30 min and the reaction rate were 71.2% and 0.041 min^{-1}, respectively; these increased with the catalyst dosage. The degradation completed in 30 min at the catalyst dosages above 0.5 g/L and the reaction rates of 0.109, 0.126, and 0.159 min^{-1} corresponding to 0.5, 0.75, and 1.0 g/L. However, the DC was decreased with increasing catalyst (Figure 11(c)).

Figure 11(d) describes the effect of catalyst dosage on degradation of TA. The increase in the dose of the catalyst increased in the active sites on the catalyst surface; the density of interaction between the irradiation and the catalytic surface increased, accelerating the generation of free radicals (•OH and $•O_2^-$). Thus, the catalytic ability of Au/ZnO was to be enhanced, whereas, as the dose of catalyst increased, the density of particles suspended on the solution increased, which will increase the effect of light scattering and interfere

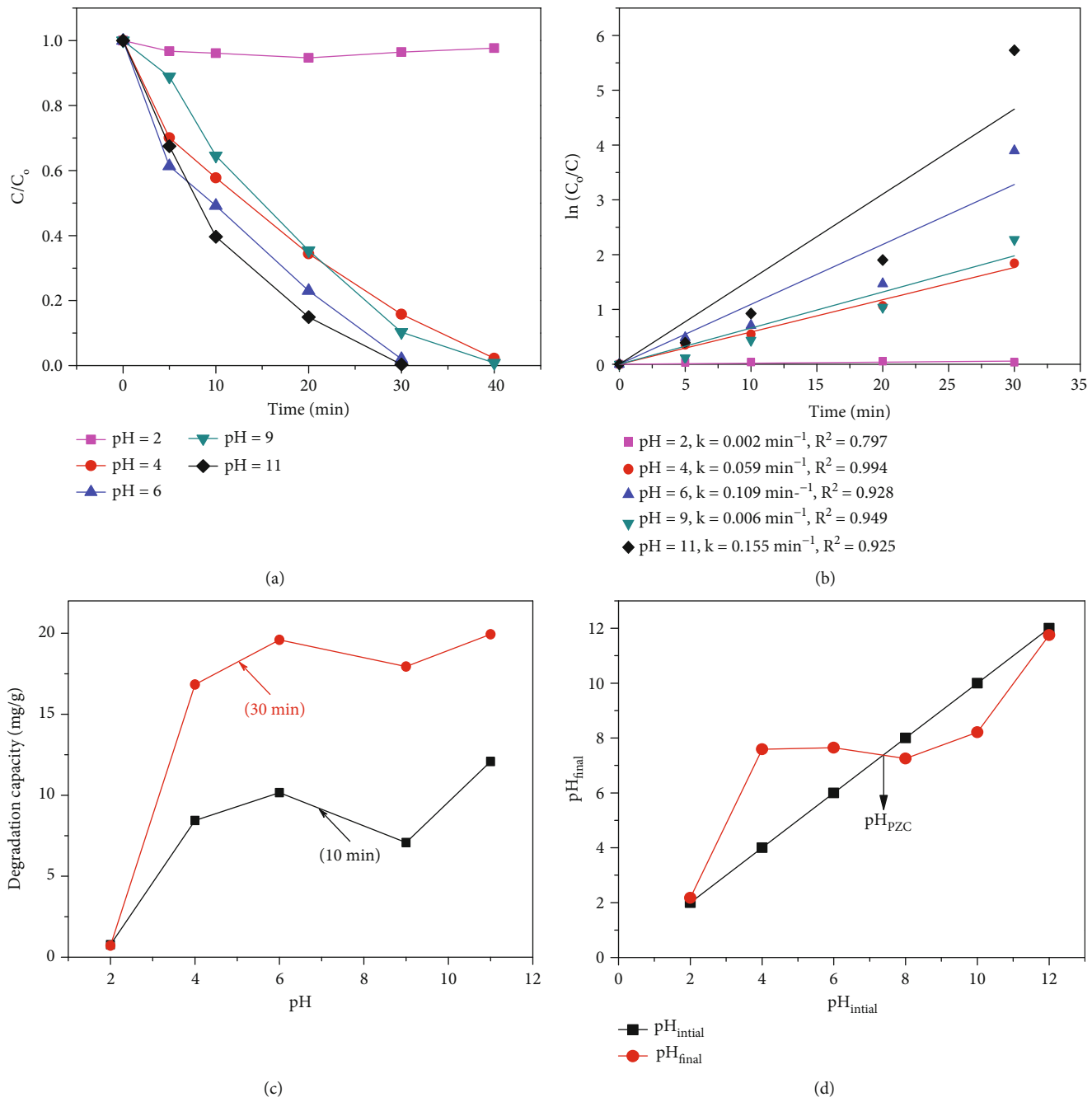

Figure 9: (a) Effect of solution pH on photodegradation of TA, (b) the kinetic curves, (c) the DC of Au/ZnO-5 composite, and (d) determination of pH_{ZPC} of Au/ZnO-5 composite. The reaction conditions: catalyst dosage of 0.5 g/L, TA concentration of 10 mg/L, and Hg lamp 250 W.

with the transmission of light deep into the solution. In addition, each catalyst site has less chance of encountering TA molecules when more catalysts were added to the reactor. As a result, DE and degradation rate could be significantly improved. However, the DC was decreased with increasing catalyst dosage.

3.2.5. Effect of Different Light Sources. The experiments were conducted under different light sources (UV lamp 15 W, Hg lamp 250 W, and sunlight). As shown in Figure 12, the reaction was strongly affected by light irradiation. The Au/ZnO-5 catalyst exhibited the best catalytic reaction with sunlight irradiation; the DE within 20 min approached 99.1% with the reaction rate of 0.176 min^{-1}. The reaction was slightly decreased with the Hg lamp but it showing significantly decreased with UV light, the DE and reaction rate were lowered to 23.2% and 0.008 min^{-1}, respectively. The low intensity of UV light, the improvement of adsorption in visible light (Figure 2(a)) with the good deposition of Au in composite, and the surface plasmonic resonance interaction of Au and ZnO particles have enhanced the catalytic performance of Au/ZnO-5 composite.

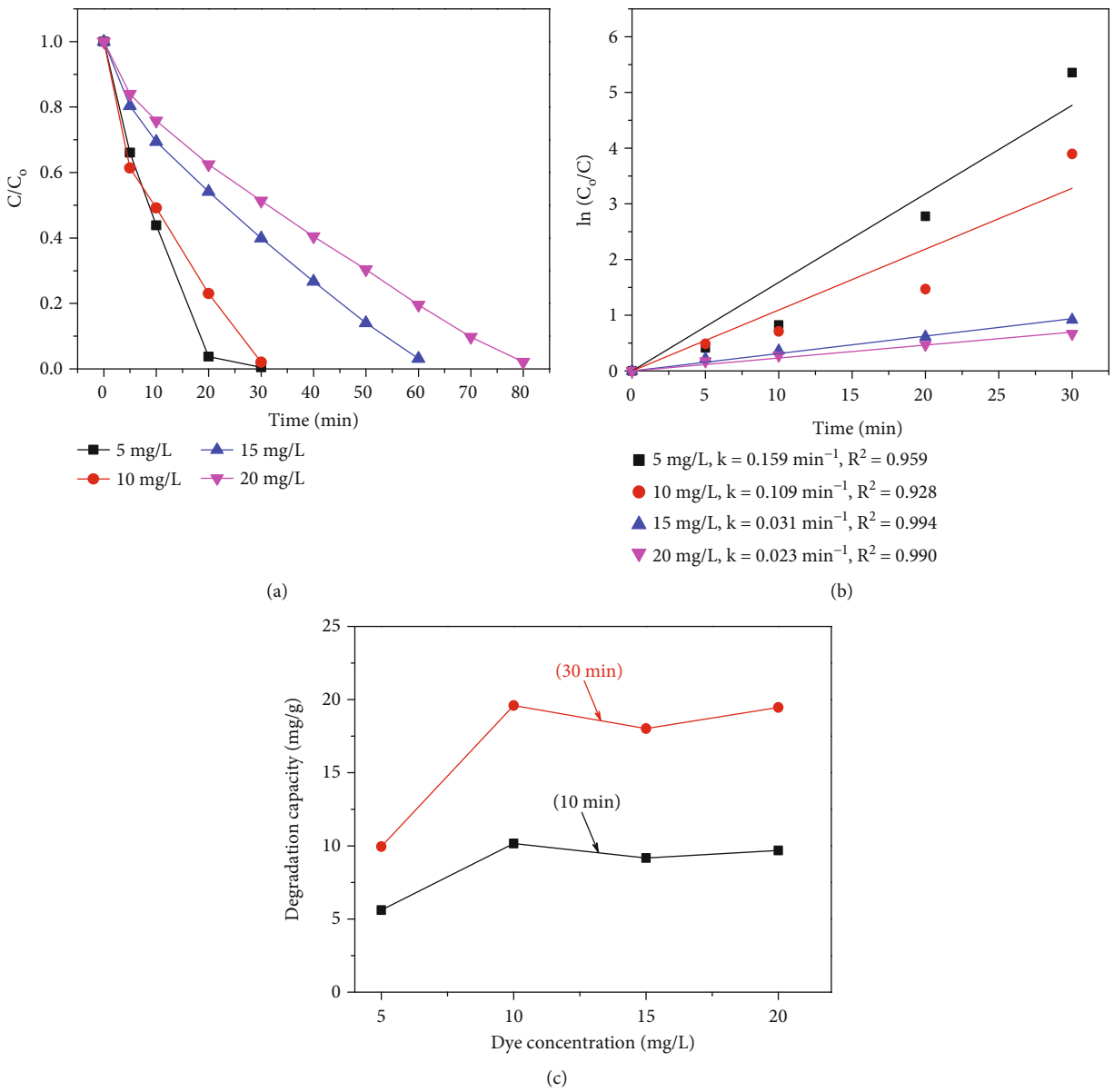

Figure 10: (a) Effect of initial TA concentration of TA on photodegradation, (b) the kinetic curves, and (c) the DC with different initial concentrations: the reaction conditions: catalyst dosage of 0.5 g/L, pH solution of 6.0, and Hg lamp 250 W.

3.2.6. Effects of Oxidizing Agents. Hydroperoxide is an oxidizing agent that can directly decompose persistent organic matter, but at a small rate, its presence can be expected to change the catalytic ability of Au/ZnO composite. The experiments were carried out in the presence of H_2O_2 at concentrations from 5 mM to 100 mM; the results are shown in Figure 13. The DE, reaction rate constant, and DC in 30 min at the H_2O_2 concentration of 5 mM were 90.4%, 0.072 min^{-1}, and 18.2 mg/g, respectively. These were slightly decreased at the concentration of 10 mM. When the concentration increased to 50 mM, the reaction rate constant increased to 0.144 min^{-1}, exhibiting the DE within 30 min of 100%. Since, the increase of the number of H_2O_2 molecules in the reaction medium could accelerate the generation of •OH radicals from either scavenging $e^-_{(CB)}$ on surface Au/ZnO-5 catalyst (Equation (5)) or absorbing the photon energy (Equation (6)), leading to an enhanced degradation process of organic matter.

$$e^-_{(CB)} + H_2O_2 \longrightarrow \bullet OH + OH^-, \quad (5)$$

$$H_2O_2 + h\nu \longrightarrow 2\bullet OH. \quad (6)$$

Further, the increase in H_2O_2 concentration to 100 mM remarkably lowered reaction. At the concentration of 100 mM, the reaction rate constant of 0.036 min^{-1} and the DE still archived 97.2% after 50 min. As the obtained results, the DCs at 50 mM were 10.4 and 20.0 mg/g in 10 and 30 min, respectively (Figure 13(c)), showing larger than other concentrations. Since, at high H_2O_2 content, the excess H_2O_2 molecules could act as an inhibitor in the generation of hydroxyl radicals, they can react with •OH and $h^+_{(VB)}$ on

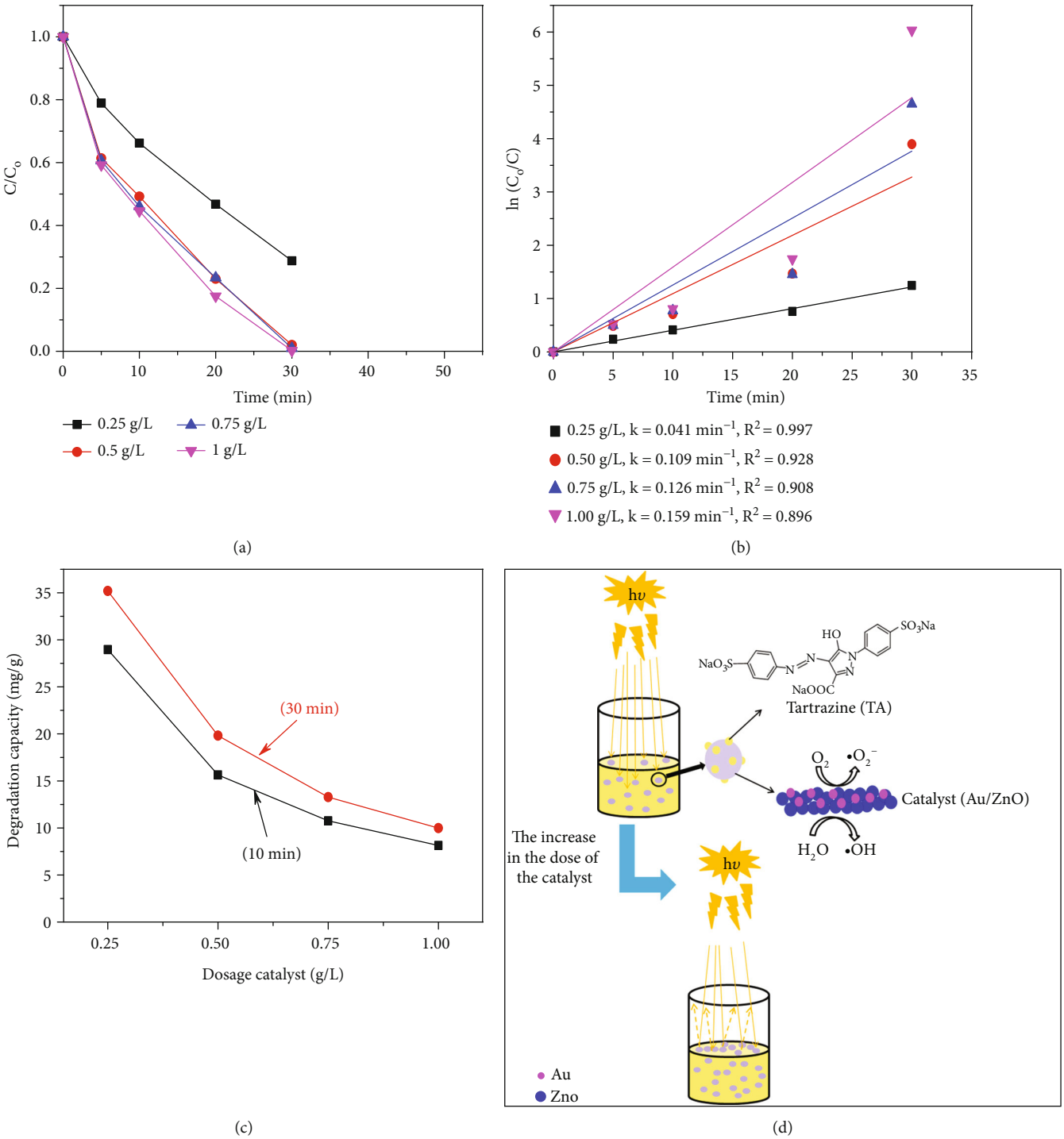

Figure 11: (a) Effect of catalyst dosage on degradation of TA, (b) the kinetic curves, (c) the DC versus dosage catalyst, and (d) schematic illustration of the effect of catalyst dosage on degradation of TA. The reaction conditions: catalyst dosage of 0.5 g/L, TA concentration of 10 mg/L, and pH solution of 6.0.

the catalyst surface to form weaker oxidizing radicals $O_2H\bullet$, as expressed in Equations (7) and (8) [48]:

$$H_2O_2 + \bullet OH \longrightarrow H_2O + O_2H\bullet \quad (7)$$

$$H_2O_2 + h^+_{(VB)} \longrightarrow H^+ + O_2H\bullet \quad (8)$$

The alternative experiment was conducted in the presence of O_2 bubbles at a flow rate of 5 mL/min. The presence of O_2 in the reaction medium can enhance the photocatalytic degradation of dyes since surface absorbed O_2 can react with electrons to produce $\bullet O^{2-}$ radicals (Equation (9)); the strong oxidizing agents can degrade dyes into CO_2 and H_2O.

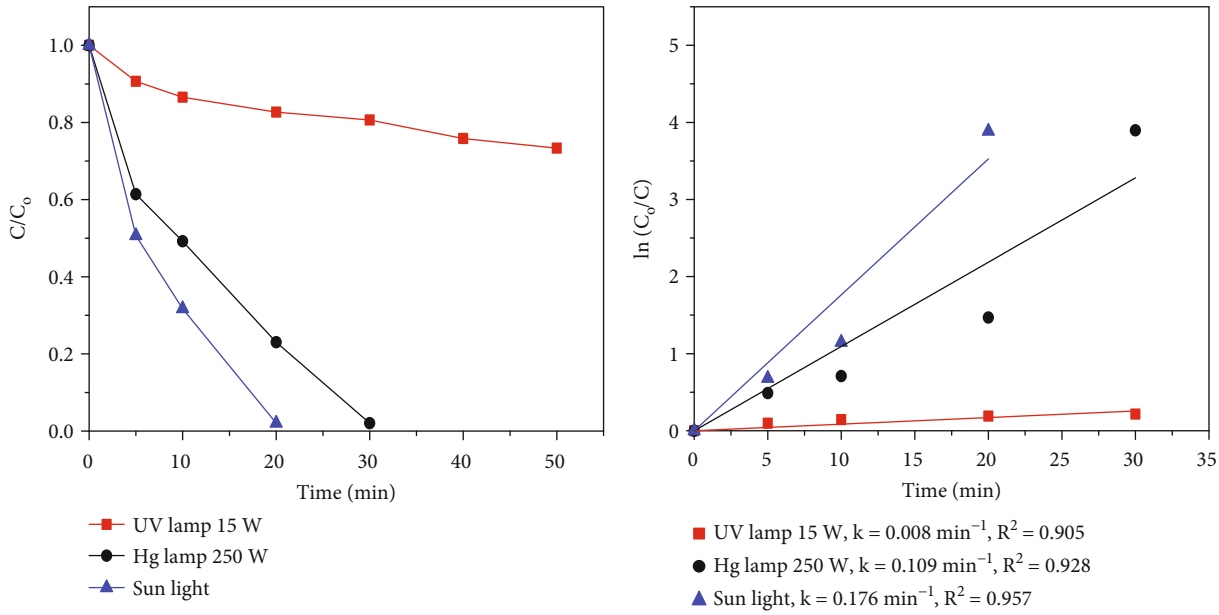

FIGURE 12: (a) Effect of different light sources on degradation of TA and (b) the kinetic curves. The reaction conditions: the reaction conditions: catalyst dosage of 0.5 g/L, TA concentration of 10 mg/L, and pH solution of 6.0.

$$O2 + e^{-}_{(CB)} \longrightarrow \bullet O_2^{-} \quad (9)$$

With adding O_2, the DE and reaction rate in the initial 10 min had no change from those without adding O_2. However, from 10 min onwards, the DC and reaction rate constant became larger than those without adding O_2, these reaching to 91.7% and 0.057 min^{-1}, respectively. However, the catalytic activity of the Au/ZnO-5 composite with the addition O_2 was still lower than that of adding H_2O_2 (Figure 14).

3.2.7. Degradation of the Different Organic Dyes Using Au/ZnO. Besides being affected by the catalytic properties (morphology, particle size, and Au/ZnO ratio) and the parameters of the catalysis process, the catalytic performance also strongly depends on the structure and bonding of the dyes. Although each catalytic process has its optimal reaction condition for degradation of a certain dye, we compared the catalytic performance of Au/ZnO-5 composite for different dyes such as methylene blue (MB), Janus Green B (JGB), and Congo red (CR) at the optimal conditions of TA. The results are presented in Figure 15. The photocatalytic degradation of CR in the Au/ZnO catalyst was very fast, showing the DE of 100% in 5 min. The degradation processes were almost complete in 30 and 40 min for TA and MB, respectively. While JGB was found to be the most difficult to degrade among the selected dyes, it showed the lowest reaction rate and DE at 30 min, which were 0.021 min^{-1} and 45.7%, respectively.

Table 1 shows a brief comparison of organic dye removal efficiency by different precious metal-doped ZnO catalysts through photocatalytic activity. The DE and reaction rate of organic dyes using the Au/ZnO-5 composite in this study under Hg lamp 250 W light irradiation were almost much higher than ZnO-based catalysts in some of the recent reports. It demonstrates that Au/ZnO is a potential catalyst in wastewater treatment.

3.3. Reaction Mechanism. Figure 16 shows the photocatalytic mechanism of dye on Au/ZnO-5 composite under visible light irradiation. When ZnO receives the energy of photons from radiation, electrons in the valence band (VB) will move to the conduction band (CB) and form pairs of electrons and holes (e^- and h^+). These excited electrons react with the adsorbed O_2 molecules on the surface of the material to generate $\bullet O_2^-$ since the bottom of the CB of ZnO (−0.5 V vs. normal hydrogen electrode, NHE) is lower than the redox potential of $O_2/\bullet O_2^-$ (−0.33 V vs. NHE). Subsequently, the formed $\bullet O_2^-$ radicals can continue to interact with H_2O to produce H_2O_2. On the other hand, the top of the VB of ZnO (+2.7 V vs. NHE) is higher than the redox potential of $\bullet OH/H_2O$, resulting in the oxidation of water molecules by these holes forming •OH radicals [49]. These powerful oxidizing agents such as H_2O_2, $\bullet O_2^-$ and •OH will attack the pollutants adsorbed on the surface of ZnO simultaneously to rapidly produce intermediate compounds and finally convert to CO_2 and H_2O (Figure 16(a)). However, the limitations of bare ZnO are the rapid decrease of catalytic activity and the low activity in the visible light region due to its extremely fast recombination of electrons and holes and poor absorption of the visible light.

When Au nanoparticles are presented in the composite, the Schottky barrier, which facilities electron capture, is formed at the interface between Au and ZnO by virtue of the fact that the work function of Au (~5.3 eV) is higher than that of ZnO (~4.2 eV) [30]. Electrons are easily

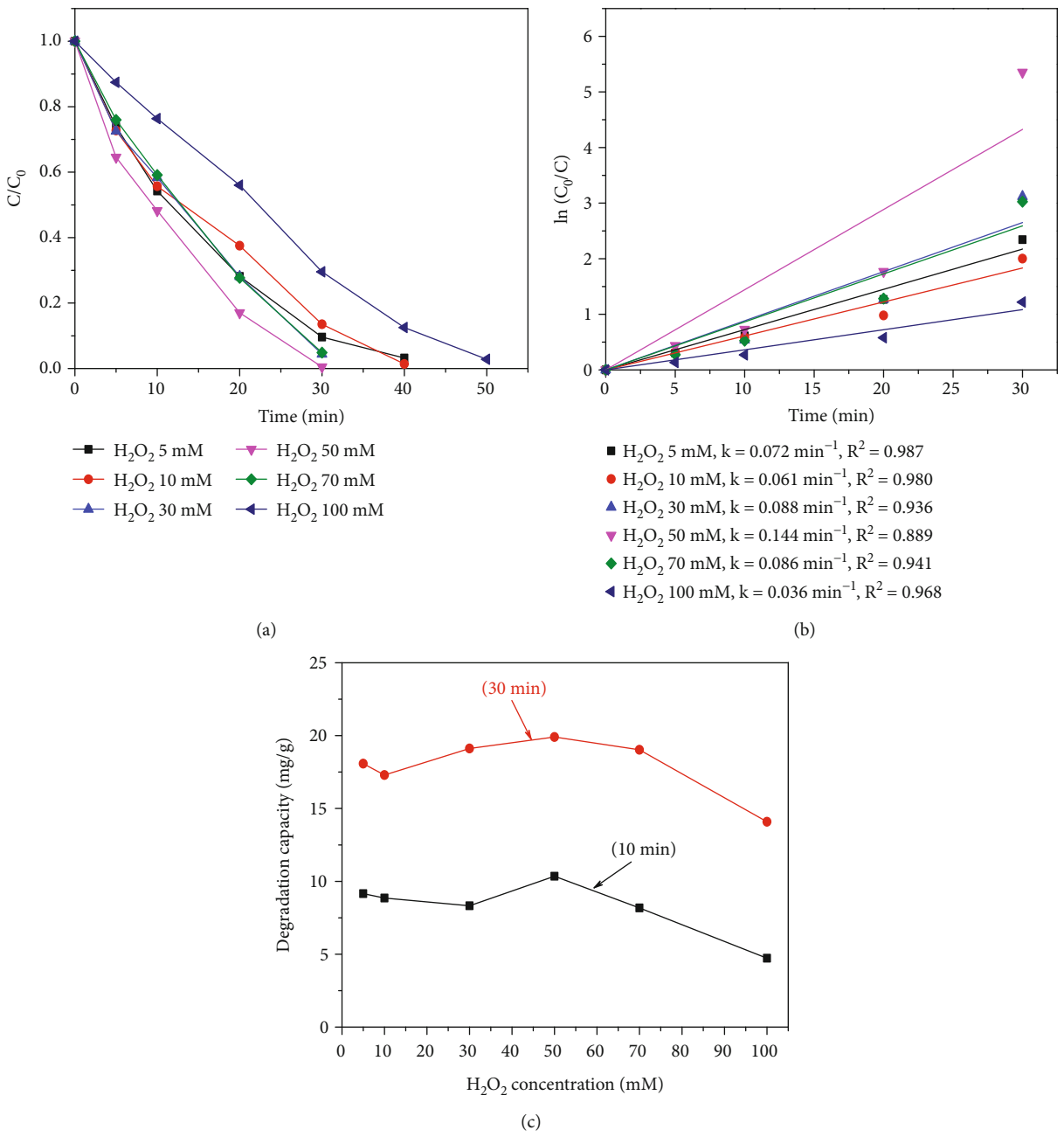

FIGURE 13: (a) Effect of initial H_2O_2 concentration on degradation of tartrazine, (b) the kinetic curves, and (c) the DC with different H_2O_2 concentrations. The reaction conditions: catalyst dosage of 0.5 g/L, TA concentration of 10 mg/L, pH solution of 6.0, and Hg lamp 250 W.

transferred from the conduction band of ZnO across the Schottky barrier to the Au nanoparticles depicted by the red arrow (Figure 16(b)). This prolongs the lifetime of charge carriers, leading to decrease the recombination of photoinduced e^- and h^+ and enhance the photocatalytic activity of ZnO. In this case, it could be seen that Au acting as an electron scavenger can trap the photogenerated electrons from the semiconductor. As a result, the accumulated electrons on Au can interact with O_2 to generate $\bullet O_2^-$ radicals, while the holes in ZnO can interact with $H_2O_2/H_2O_2/OH^-$ to generate •OH radicals to degrade the organic pollutants. This also explains the enhancement of catalytic performance in the presence of O_2 and H_2O_2 in the reaction medium. These processes are described by the following equations:

$$\begin{aligned}
\mathrm{ZnO} + h\nu &\longrightarrow \mathrm{ZnO}(e^-) + h^+ \\
\mathrm{ZnO}\,(e^-) + \mathrm{Au} &\longrightarrow \mathrm{ZnO} + \mathrm{Ag}\,(e^-) \\
\mathrm{Au}(e^-) + \mathrm{O_2} &\longrightarrow \bullet\mathrm{O_2^-} + \mathrm{Au} \\
\mathrm{ZnO}\left(h^+\right) + \mathrm{H_2O} &\longrightarrow \mathrm{ZnO} + \mathrm{H^+} + \bullet\mathrm{OH} \\
(\bullet\mathrm{O_2^-} + \bullet\mathrm{OH}) + \text{organic dyes} &\longrightarrow \text{Intermediate products} \\
(\bullet\mathrm{O_2^-} + \bullet\mathrm{OH}) + \text{Intermediate products} &\longrightarrow \mathrm{CO_2} + \mathrm{H_2O}
\end{aligned} \tag{10}$$

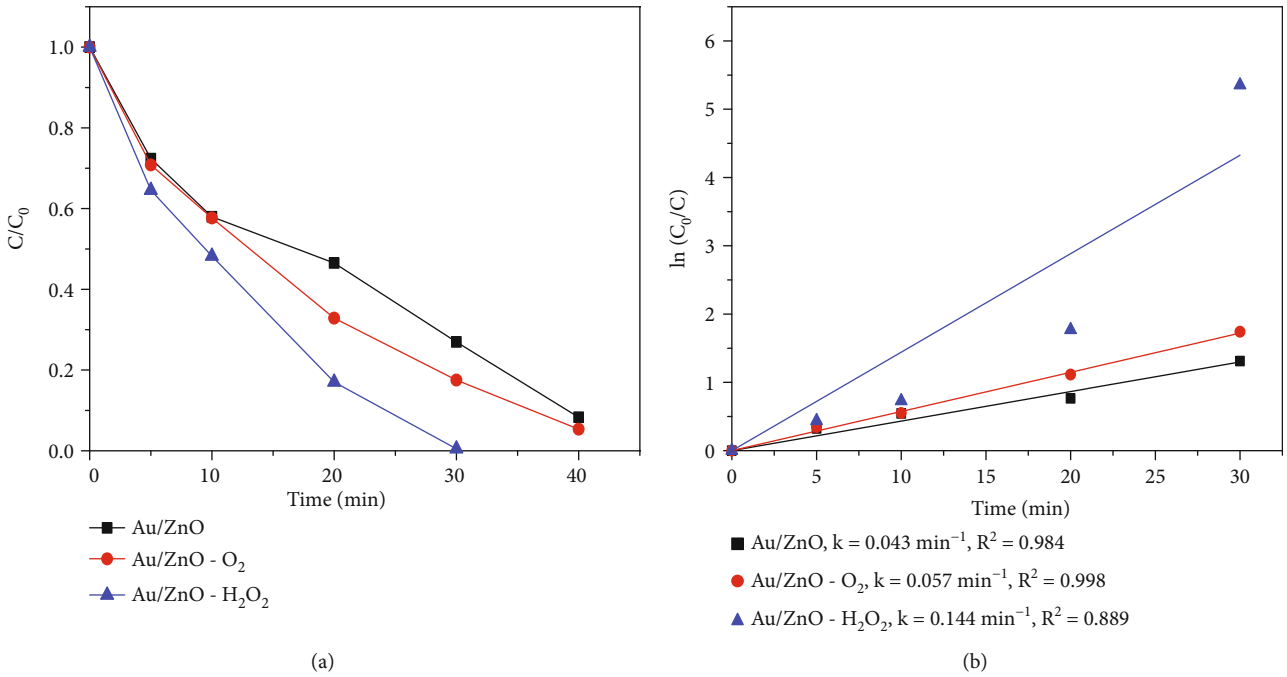

Figure 14: (a) Effect of oxidizing agent on degradation of TA and (b) the kinetic curves. The reaction conditions: catalyst dosage of 0.5 g/L, TA concentration of 10 mg/L, pH solution of 6.0, and Hg lamp 250 W.

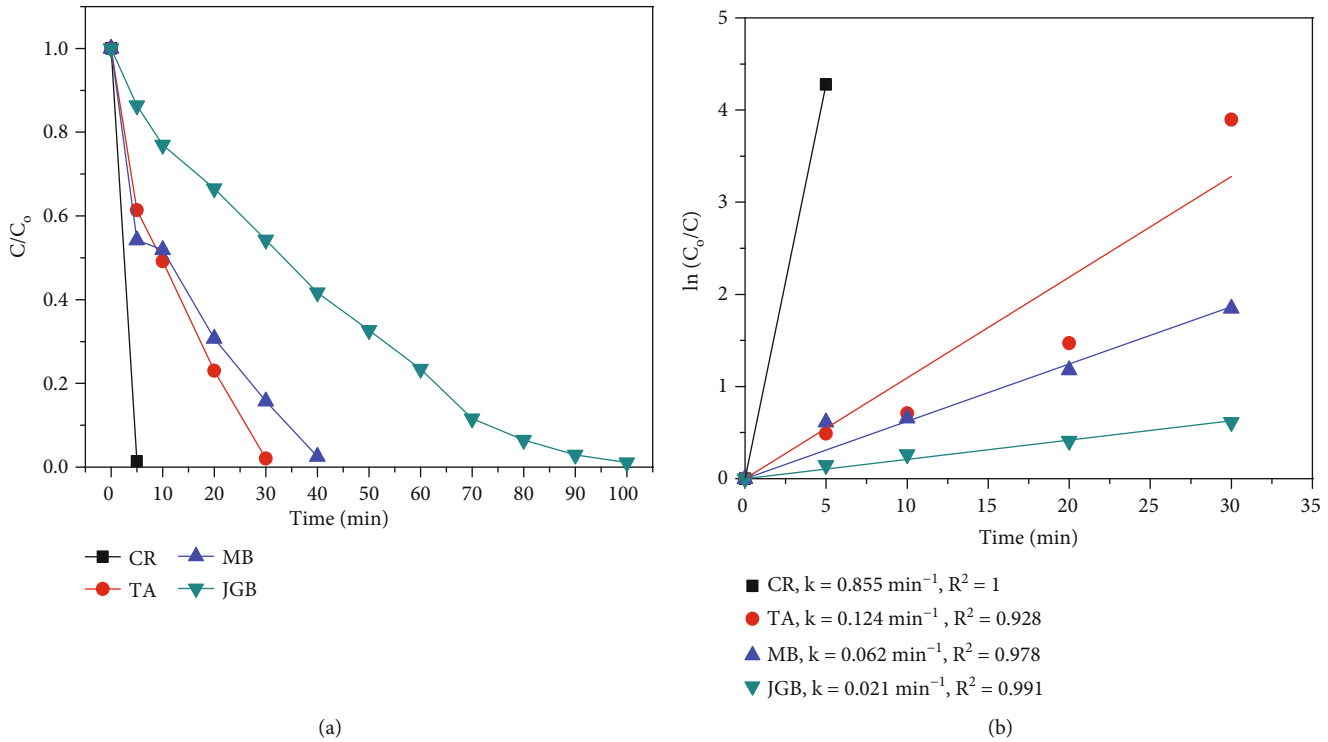

Figure 15: (a) Degradation of the different organic dyes on Au/ZnO-5 composite; (b) the kinetic curves. The reaction conditions: catalyst dosage of 0.5 g/L, dyes concentration of 10 mg/L, solution pH of 6.0, and Hg lamp of 250 W.

Alternatively, several studies have demonstrated that Au and Ag nanoscales (size below 10 nm) in composites could induce surface plasmon resonance (SPR) [50–52]. It is the strong oscillation of the free electrons in the metal in phase with the electric field of the shining light [26]. Besides metal-semiconductor junction, the localized surface plasmon resonance can provide semiconductor materials with favorable properties for photocatalysis such as visible light response, which enhanced UV/vis absorption, reduced e^-/h^+ diffusion length, and enhanced local electric field. Also,

Table 1: Comparison of photocatalytic degradation of different organic dyes using precious metal-doped ZnO nanocomposites.

Catalyst, dosage (g/L)	Target pollutant (concentration, mg/L)	Light source	Degradation time/efficiency	Reaction rate, k (min^{-1})	Reference
Au (5 wt%)/ZnO, 0.5 g/L	CR (16 mg/L)	UV lamp 100 W	60 min/77.2%	0.0196 min^{-1}	
Ag (5 wt%)/ZnO, 0.5 g/L	CR (16 mg/L)	UV lamp 100 W	60 min/81.2%	0.0226 min^{-1}	[30]
Pd (5 wt%)/ZnO, 0.5 g/L	CR (16 mg/L)	UV lamp 100 W	60 min/98.2%	0.0576 min^{-1}	
Au/ZnO-5, 0.5 g/L	CR (10 mg/L)	Hg lamp 250 W	5 min/100%	0.855 min^{-1}	This work
ZnO/Au15 (15 wt%), 0.5 g/L	MB (10 mg/L)	Xenon lamp 100 W	120 min/90%	0.0182 min^{-1}	[54]
Ag-Cu-ZnO (2 : 2 : 96 wt%), 1 g/L	MB (10 mg/L)	Tungsten lamp 400 W	180 min/95%	0.0111 min^{-1}	[55]
Au/ZnO-5, 0.5 g/L	MB (10 mg/L)	Hg lamp 250 W	40 min/98,7%	0.062 min^{-1}	This work
Ag (10%wt)/ZnO, 0.5 g/L	JGB (10 mg/L)	Solar light	60 min/83%	0.028 min^{-1}	[23]
Au/ZnO-5, 0.5 g/L	JGB (10 mg/L)	Hg lamp 250 W	100 min/99.5%	0.021 min^{-1}	This work
Ag (3 wt%)/ZnO, 0.2 g/L	TA (25 mg/L)	Hg lamp 8 W	60 min/95.2%	0.0497 min^{-1}	[33]
Au/ZnO-5, 0.5 g/L	TA (10 mg/L)	Hg lamp 250 W	30 min/99.2%	0.109 min^{-1}	This work

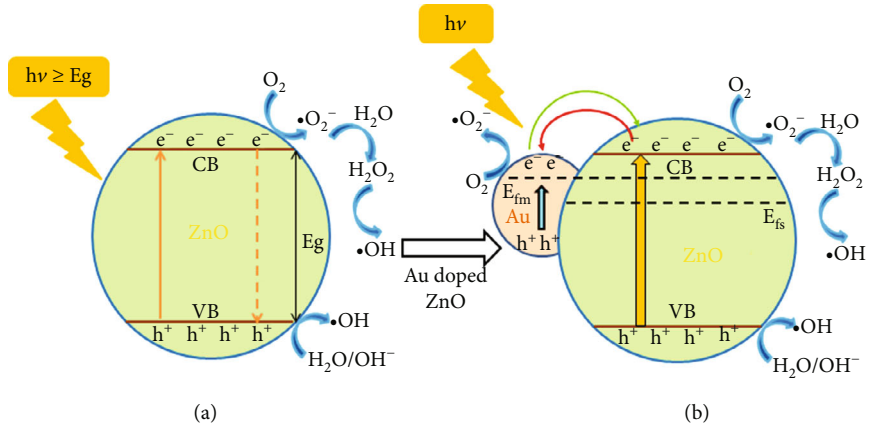

Figure 16: Schematic model for the photocatalytic mechanism of (a) bare ZnO and (b) Au/ZnO composite.

they have been investigated in XRD, DR/UV-Vis, and EPR analyses. The significant enhancement of wavelength absorption with low-bandgap photocatalyst and ultraviolet absorption of wide-bandgap photocatalyst, the inhibition of electron transfer from nano Au to ZnO (green arrow in Figure 16(b)), and the enhancement of electron transport capacity due to strong absorption of incident radiation in the thin layer (~10 nm) below the catalyst surface lead to the enhanced photocatalytic performance of the Au/ZnO-5 composite.

In this study, tartrazine was selected as a typical pollutant model for investigating the photocatalytic efficiency of Au/ZnO nanocomposite. Tartrazine is a synthetic lemon yellow azo dye; it exists in three conformational forms depending on the solution pH (azo, keto, and hydrazone form as shown in Figure 17(a)). At pH = 6, tartrazine has two forms as azo and keto form; meanwhile, all three forms above are in being at pH = 11 [53]. A suitable photocatalytic degradation pathway of TA with Au/ZnO catalyst was proposed in Figure 17(b), which describes the breaking of functional groups, bonds, and azo groups by oxidizing agents and giving rise to intermediate products, ultimately CO_2, SO2, Na_2CO_3, etc.

4. Conclusion

Hierarchical structure Au/ZnO composite was successfully synthesized by the hydrothermal method and chemical reduction by sodium citrate. Au/ZnO-5 composite was a hierarchical structure like flowers. The ZnO particles were approximately 10-15 μm in size, which were composed of many petals. The Au particles of 3-5 nm in size were well dispersed on the ZnO structure, which was observed in EDS, TEM, and EPR results. The presence of Au at a higher 3 wt.% led to reducing the bandgap energy to 3.12 eV but slightly increasing the crystal size to 15 nm for Au/ZnO-5 composite. In addition, the presence of Au led to a decrease in the strength of an EPR signal for Au/ZnO-5 composite; it promoted the transfer of electrons from Au to ZnO and subsequently paired with the single electron in Vo•, resulting in the formation of paramagnetically silent Vo••. These were the reasons for the reduction of the recombination of electrons and holes. Therefore, the photocatalytic ability of Au/ZnO composite was improved. Moreover, the enhanced photocatalytic performance of composite under sunlight irradiation with doping of Au could be attributed to the surface plasmonic resonance interaction of Au and ZnO

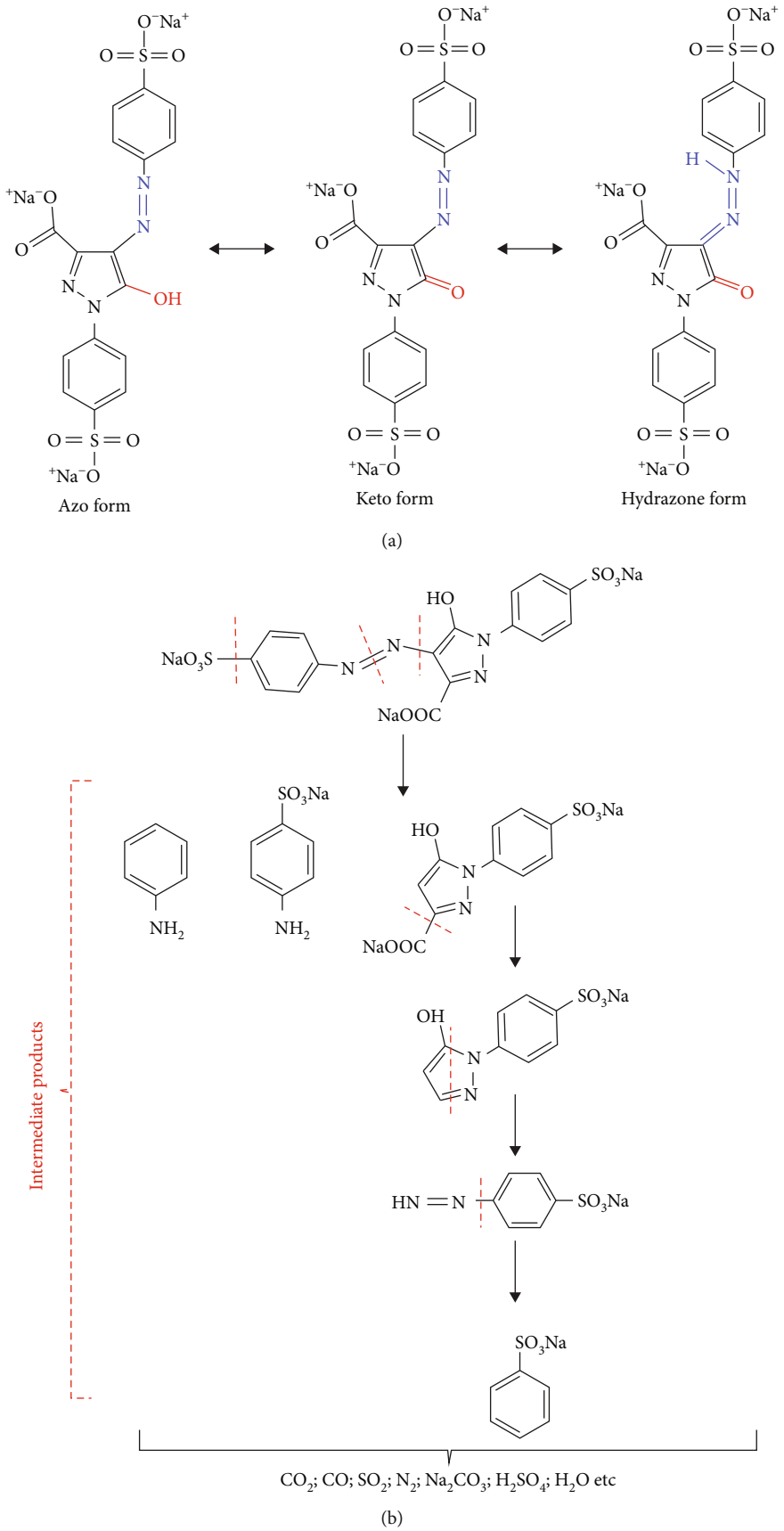

Figure 17: (a) The tautomeric forms of tartrazine and (b) possible route to the destruction of tartrazine in as-synthesized Au/ZnO nanocomposite.

particles and the intensity of sunlight. As the results, the Au/ZnO-5 composite exhibited a high reaction activity. Its DE, reaction rate, and DC were 99.2%, 0.109 min^{-1}, and 19.6 mg/g, respectively.

The pH of 6.0, dye concentration of 10 mg/L, and catalyst dosage of 0.25 g/L were potential conditions for the degradation of dye on Au/ZnO-5 composite. The presence of O_2 and H_2O_2 could accelerate the generation of •OH and $•O_2^-$ radicals leading to improve degradation of dyes into CO_2 and H_2O. However, at a high concentration of H_2O_2 (above 100 mM), the reaction was drastically reduced because that H_2O_2 acted as a scavenger to •OH radicals. In addition, the Au/ZnO-5 composite also exhibited an excellent catalyst for other dyes showing degradation of 100% in 5 min for Congo red.

Data Availability

The research data used to support the findings of this study are included within the article.

Conflicts of Interest

The authors declare that they have no conflicts of interest.

Acknowledgments

The authors are grateful for the financial support from the Vietnam National Foundation for Science and Technology Development (NAFOSTED) under grant number 104.05-2018.333 and Hanoi University of Industry (HaUI) under grant number 18-2020-RD/HĐ-ĐHCN. Pham Thi Anh Tuyet was funded by Vingroup Joint Stock Company and supported by the Domestic Master/PhD Scholarship Programme of Vingroup Innovation Foundation (VINIF), Vingroup Big Data Institute (VINBIGDATA), code VINIF.2020.ThS.18.

References

[1] G. Sharma, A. García-Peñas, M. Naushad, A. Kumar, M. Sillanpää, and F. J. Stadler, "Trimetallic@ cyclodextrin nanocomposite: photocatalyst for degradation of amoxicillin and catalyst for esterification reactions," *Journal of Chemistry*, vol. 2021, Article ID 5512563, 2021.

[2] V. Amendola, R. Pilot, M. Frasconi, O. M. Maragò, and M. A. Iatì, "Surface plasmon resonance in gold nanoparticles: a review," *Journal of Physics: Condensed Matter*, vol. 29, no. 20, article 203002, 2017.

[3] I. Khan, K. Saeed, and I. Khan, "Nanoparticles: properties, applications and toxicities," *Arabian Journal of Chemistry*, vol. 12, no. 7, pp. 908–931, 2019.

[4] P. Suchomel, L. Kvitek, R. Prucek et al., "Simple size-controlled synthesis of Au nanoparticles and their size- dependent catalytic activity," *Scientific Reports*, vol. 8, no. 1, p. 4589, 2018.

[5] D. A. Boyne, A. M. Savage, M. H. Griep, F. L. Beyer, and J. A. Orlicki, "Process induced alignment of gold nano-rods (GNRs) in thermoplastic polymer composites with tailored optical properties," *Polymer*, vol. 110, pp. 250–259, 2017.

[6] L. C. du, W. D. Xi, J. B. Zhang, H. Matsuzaki, and A. Furube, "Electron transfer dynamics and yield from gold nanoparticle to different semiconductors induced by plasmon band excitation," *Chemical Physics Letters*, vol. 701, pp. 126–130, 2018.

[7] R. Wang, J. Deng, D. He et al., "Corrigendum to "PEGylated hollow gold nanoparticles for combined X-ray radiation and photothermal therapy in vitro and enhanced CT imaging"," *Nanomedicine: Nanotechnology, Biology and Medicine*, vol. 16, article 102313, pp. 195–205, 2020.

[8] H. T. Thu, L. T. Dat, and V. A. Tuan, "Synthesis of mesoporous SiO_2 from rice husk for removal of organic dyes in aqueous solution," *Vietnam Journal of Chemistry*, vol. 57, no. 2, pp. 175–181, 2019.

[9] C. Zhao, J. Zhou, Y. Yan et al., "Application of coagulation/flocculation in oily wastewater treatment: a review," *Science of The Total Environment*, vol. 765, article 142795, 2020.

[10] A.-T. Vu, T. N. Xuan, and C.-H. Lee, "Preparation of mesoporous Fe_2O_3·SiO_2 composite from rice husk as an efficient heterogeneous Fenton-like catalyst for degradation of organic dyes," *Journal of Water Process Engineering*, vol. 28, pp. 169–180, 2019.

[11] P. Anukorn, P. Prapassornwattana, S. Thongtem, and T. Thongtem, "Synthesis of heterostructure Au/ZnO nanocomposites by microwave-assisted deposition method and their photocatalytic activity in methylene blue degradation," *Russian Journal of Physical Chemistry A*, vol. 94, no. 7, pp. 1464–1470, 2020.

[12] S. Sharma, V. Dutta, P. Singh et al., "Carbon quantum dot supported semiconductor photocatalysts for efficient degradation of organic pollutants in water: a review," *Journal of Cleaner Production*, vol. 228, pp. 755–769, 2019.

[13] A. Kumar, G. Sharma, M. Naushad et al., "Bio-inspired and biomaterials-based hybrid photocatalysts for environmental detoxification: a review," *Chemical Engineering Journal*, vol. 382, p. 122937, 2020.

[14] N. L. Gavade, A. N. Kadam, S. B. Babar, A. D. Gophane, K. M. Garadkar, and S. W. Lee, "Biogenic synthesis of gold-anchored ZnO nanorods as photocatalyst for sunlight-induced degradation of dye effluent and its toxicity assessment," *Ceramics International*, vol. 46, no. 8, pp. 11317–11327, 2020.

[15] M. Pirhashemi and A. Habibi-Yangjeh, "Facile fabrication of novel ZnO/$CoMoO_4$ nanocomposites: highly efficient visible-light-responsive photocatalysts in degradations of different contaminants," *Journal of Photochemistry and Photobiology A: Chemistry*, vol. 363, pp. 31–43, 2018.

[16] J. Lu, H. Wang, D. Peng, T. Chen, S. Dong, and Y. Chang, "Synthesis and properties of Au/ZnO nanorods as a plasmonic photocatalyst," *Physica E: Low-dimensional Systems and Nanostructures*, vol. 78, pp. 41–48, 2016.

[17] Y.-F. Cheng, W. Jiao, Q. Li et al., "Two hybrid Au-ZnO aggregates with different hierarchical structures: a comparable study in photocatalysis," *Journal of Colloid and Interface Science*, vol. 509, pp. 58–67, 2018.

[18] Y. Cheng, W. Wang, L. Yao, J. Wang, Y. Liang, and J. Fu, "Insights into charge transfer and solar light photocatalytic activity induced by the synergistic effect of defect state and plasmon in Au nanoparticle- decorated hierarchical 3D porous ZnO microspheres," *Applied Surface Science*, vol. 494, pp. 959–968, 2019.

[19] S. Pyne, G. P. Sahoo, D. K. Bhui et al., "Enhanced photocatalytic activity of metal coated ZnO nanowires," *Spectrochimica*

Acta Part A: Molecular and Biomolecular Spectroscopy, vol. 93, pp. 100–105, 2012.

[20] G. Shi, Q. Chen, Q. Zhang et al., "Morphology effect of ZnO support on the performance of Cu toward methanol production from CO_2 hydrogenation," *Journal of Saudi Chemical Society*, vol. 24, no. 1, pp. 42–51, 2020.

[21] R. Mohan, K. Krishnamoorthy, and S.-J. Kim, "Diameter dependent photocatalytic activity of ZnO nanowires grown by vapor transport technique," *Chemical Physics Letters*, vol. 539-540, pp. 83–88, 2012.

[22] S. M. Saleh, "ZnO nanospheres based simple hydrothermal route for photocatalytic degradation of azo dye," *Spectrochimica Acta Part A: Molecular and Biomolecular Spectroscopy*, vol. 211, pp. 141–147, 2019.

[23] A. T. Vu, T. A. Pham, T. T. Tran et al., "Synthesis of nanoflakes Ag•ZnO•activated carbon composite from rice husk as a photocatalyst under solar light," *Bulletin of Chemical Reaction Engineering & Catalysis*, vol. 15, p. 16, 2020.

[24] L. T. Mai, L. T. Hoai, and V. A. Tuan, "Effects of reaction parameters on photodegradation of caffeine over hierarchical flower-like ZnO nanostructure," *Vietnam Journal of Chemistry*, vol. 56, no. 5, pp. 647–653, 2018.

[25] P. Li, Z. Wei, T. Wu, Q. Peng, and Y. Li, "Au–ZnO hybrid nanopyramids and their photocatalytic properties," *Journal of the American Chemical Society*, vol. 133, no. 15, pp. 5660–5663, 2011.

[26] T. A. Pham, V. A. Tran, N. M. V. Le VD, D. D. Truong, and V. A. T. Do XT, "Facile preparation of ZnO nanoparticles and Ag/ZnO nanocomposite and their photocatalytic activities under visible light," *International Journal of Photoenergy*, vol. 2020, 2020.

[27] T. V. Anh, T. A. T. Pham, V. H. Mac, and T. H. Nguyen, "Facile controlling of the physical properties of zinc oxide and its application to enhanced photocatalysis," *Journal of Analytical Methods in Chemistry*, vol. 2021, Article ID 5533734, 2021.

[28] R. Lamba, A. Umar, S. K. Mehta, and S. K. Kansal, "ZnO doped SnO_2 nanoparticles heterojunction photo-catalyst for environmental remediation," *Journal of Alloys and Compounds*, vol. 653, pp. 327–333, 2015.

[29] A. E. Ramírez, M. Montero-Muñoz, L. L. López et al., "Significantly enhancement of sunlight photocatalytic performance of ZnO by doping with transition metal oxides," *Scientific Reports*, vol. 11, no. 1, p. 2804, 2021.

[30] N. Güy and M. Özacar, "The influence of noble metals on photocatalytic activity of ZnO for Congo red degradation," *International Journal of Hydrogen Energy*, vol. 41, no. 44, pp. 20100–20112, 2016.

[31] H. Liu, J. Feng, and W. Jie, "A review of noble metal (Pd, Ag, Pt, Au)–zinc oxide nanocomposites: synthesis, structures and applications," *Journal of Materials Science: Materials in Electronics*, vol. 28, no. 22, pp. 16585–16597, 2017.

[32] H. Bouzid, M. Faisal, F. A. Harraz, S. A. al-Sayari, and A. A. Ismail, "Synthesis of mesoporous Ag/ZnO nanocrystals with enhanced photocatalytic activity," *Catalysis Today*, vol. 252, pp. 20–26, 2015.

[33] Ş. Ş. Türkyılmaz, N. Güy, and M. Özacar, "Photocatalytic efficiencies of Ni, Mn, Fe and Ag doped ZnO nanostructures synthesized by hydrothermal method: the synergistic/antagonistic effect between ZnO and metals," *Journal of Photochemistry and Photobiology A: Chemistry*, vol. 341, pp. 39–50, 2017.

[34] D. Sharma and R. Jha, "Transition metal (Co, Mn) co-doped ZnO nanoparticles: effect on structural and optical properties," *Journal of Alloys and Compounds*, vol. 698, pp. 532–538, 2017.

[35] V. Kumari, A. Mittal, J. Jindal, S. Yadav, and N. Kumar, "S-, N- and C-doped ZnO as semiconductor photocatalysts: a review," *Frontiers of Materials Science*, vol. 13, no. 1, pp. 1–22, 2019.

[36] M. S. Jyothi, V. Nayak, K. R. Reddy et al., "Non-metal (oxygen, sulphur, nitrogen, boron and phosphorus)-doped metal oxide hybrid nanostructures as highly efficient photocatalysts for water treatment and hydrogen generation," in *Nanophotocatalysis and Environmental Applications: Materials and Technology*, S. G. Inamuddin, A. Kumar, E. Lichtfouse, and A. M. Asiri, Eds., pp. 83–105, Springer International Publishing, Cham, 2019.

[37] S. G. Kumar and K. S. R. K. Rao, "Comparison of modification strategies towards enhanced charge carrier separation and photocatalytic degradation activity of metal oxide semiconductors (TiO_2, WO_3 and ZnO)," *Applied Surface Science*, vol. 391, pp. 124–148, 2017.

[38] L. T. Dat, N. T. Hung, and V. A. Tuan, "Preparation of flower-like Cu_2O/ZnO for removal of dyes from aqueous medium," *Vietnam Journal of Chemistry*, vol. 58, no. 4, pp. 517–525, 2020.

[39] G. Wu, G. Zhao, J. Sun et al., "The effect of oxygen vacancies in ZnO at an Au/ZnO interface on its catalytic selective oxidation of glycerol," *Journal of Catalysis*, vol. 377, pp. 271–282, 2019.

[40] Z. Han, L. Wei, Z. Zhang, X. Zhang, H. Pan, and J. Chen, "Visible-light photocatalytic application of hierarchical Au-ZnO flower-rod heterostructures via surface plasmon resonance," *Plasmonics*, vol. 8, no. 2, pp. 1193–1202, 2013.

[41] Y. Zhang, J. Zhou, Z. Li, and Q. Feng, "Photodegradation pathway of rhodamine B with novel Au nanorods @ ZnO microspheres driven by visible light irradiation," *Journal of Materials Science*, vol. 53, no. 5, pp. 3149–3162, 2018.

[42] M. Ahmad, E. Ahmed, Z. L. Hong, W. Ahmed, A. Elhissi, and N. R. Khalid, "Photocatalytic, sonocatalytic and sonophotocatalytic degradation of rhodamine B using ZnO/CNTs composites photocatalysts," *Ultrasonics Sonochemistry*, vol. 21, no. 2, pp. 761–773, 2014.

[43] W. E. Mahmoud, A. A. Al-Ghamdi, S. Al-Heniti, and S. Al-Ameer, "The influence of temperature on the structure of Cd-doped ZnO nanopowders," *Journal of Alloys and Compounds*, vol. 491, no. 1, pp. 742–746, 2010.

[44] M. Yang, S. Zhang, F. Qu et al., "High performance acetone sensor based on ZnO nanorods modified by Au nanoparticles," *Journal of Alloys and Compounds*, vol. 797, pp. 246–252, 2019.

[45] J. H. Park, G. Choppala, S. J. Lee, N. Bolan, J. W. Chung, and M. Edraki, "Comparative sorption of Pb and Cd by biochars and its implication for metal immobilization in soils," *Water, Air, & Soil Pollution*, vol. 224, no. 12, p. 1711, 2013.

[46] X. Liu, M.-H. Liu, Y.-C. Luo et al., "Strong metal–support interactions between gold nanoparticles and ZnO nanorods in CO oxidation," *Journal of the American Chemical Society*, vol. 134, no. 24, pp. 10251–10258, 2012.

[47] C. Yang, J. Yu, Q. Li, and Y. Yu, "Facile synthesis of monodisperse porous ZnO nanospheres for organic pollutant degradation under simulated sunlight irradiation: the effect of operational parameters," *Materials Research Bulletin*, vol. 87, pp. 72–83, 2017.

[48] M. A. Behnajady, N. Modirshahla, and R. Hamzavi, "Kinetic study on photocatalytic degradation of C.I. Acid Yellow 23

by ZnO photocatalyst," *Journal of Hazardous Materials*, vol. 133, no. 1, pp. 226–232, 2006.

[49] K. Qi, B. Cheng, J. Yu, and W. Ho, "Review on the improvement of the photocatalytic and antibacterial activities of ZnO," *Journal of Alloys and Compounds*, vol. 727, pp. 792–820, 2017.

[50] W. Li, F. Hua, J. Yue, and J. Li, "Ag@AgCl plasmon-induced sensitized ZnO particle for high-efficiency photocatalytic property under visible light," *Applied Surface Science*, vol. 285, pp. 490–497, 2013.

[51] S.-i. Naya, T. Nikawa, K. Kimura, and H. Tada, "Rapid and complete removal of nonylphenol by gold nanoparticle/rutile titanium(IV) oxide plasmon photocatalyst," *ACS Catalysis*, vol. 3, no. 5, pp. 903–907, 2013.

[52] H. Liu, Y. Hu, Z. Zhang, X. Liu, H. Jia, and B. Xu, "Synthesis of spherical Ag/ZnO heterostructural composites with excellent photocatalytic activity under visible light and UV irradiation," *Applied Surface Science*, vol. 355, pp. 644–652, 2015.

[53] M. G. Popadić, S. R. Marinović, T. M. Mudrinić et al., "A novel approach in revealing mechanisms and particular step predictors of pH dependent tartrazine catalytic degradation in presence of Oxone®," *Chemosphere*, vol. 281, p. 130806, 2021.

[54] S. S. Naik, S. J. Lee, T. Begildayeva, Y. Yu, H. Lee, and M. Y. Choi, "Pulsed laser synthesis of reduced graphene oxide supported ZnO/Au nanostructures in liquid with enhanced solar light photocatalytic activity," *Environmental Pollution*, vol. 266, p. 115247, 2020.

[55] M. Rabbani, J. Shokrayian, R. Rahimi, and R. Amrollahi, "Comparison of photocatalytic activity of ZnO, Ag-ZnO, Cu-ZnO, Ag, Cu-ZnO and TPPS/ZnO for the degradation of methylene blue under UV and visible light irradiation," *Water Science and Technology*, vol. 84, no. 7, pp. 1813–1825, 2021.